High pressure partitioning behavior of Mo and W and late sulfur delivery during Earth's core formation

Dongyang Huang, Julien Siebert, James Badro

High pressure partitioning behavior of Mo and W and late sulfur delivery during Earth's core formation

Dongyang Huang[a], Julien Siebert[a,b], James Badro[a]

[a] *Université de Paris, Institut de Physique du Globe de Paris, 75005 Paris, France*
[b] *Institut Universitaire de France, France*

Abstract

Mo and W in the bulk silicate Earth and their partitioning behavior between molten metal and silicate can be used to constrain the thermochemical conditions during Earth's core-mantle differentiation. In order to improve our understanding of core-forming conditions, we performed a series of superliquidus metal-silicate partitioning experiments on Mo and W at 40-93 GPa and 3000-4700 K in laser-heated diamond anvil cells. Under the extended P-T conditions directly relevant to terrestrial core formation in a deep magma ocean, we find that pressure and temperature have profound yet opposing effects on their partitioning, and a significant amount of O dissolved in the metal. Based on an activity model for liquid Fe-rich metal, it is observed that O enhances the solubility of both Mo and W in the metal, whereas S makes W significantly less siderophile than Mo. Combining our new data with those of the literature, we modeled the effects of pressure, temperature and metal composition on partitioning, and applied them to a multi-stage accretion model. While our model with homogeneous S accretion successfully explains the abundance of Mo, it underestimates that of W and therefore overestimates Mo/W ratio in Earth's mantle, regardless of the oxidation conditions prevailing during core formation. On the other hand, mantle observables (Mo and W abundances, Mo/W ratio) can be reproduced simultaneously if S is supplied to the Earth towards the end of accretion. This corroborates previous work at lower pressures, and agrees with heterogeneous accretion models where the late volatile-rich delivery was envisaged to explain various isotopic signatures of terrestrial bodies. Nonetheless, this conclusion does not discriminate between reducing and oxidizing conditions.

Email address: huang@ipgp.fr (Dongyang Huang)

Keywords: Core formation, siderophile elements, Mo/W ratio, volatile delivery, metal-silicate partitioning, high pressure

1. Introduction

Core formation by metal-silicate segregation in a magma ocean is the first significant differentiation event in Earth (Ringwood, 1959; Li and Agee, 1996; Wood et al., 2006). This equilibration process partitions siderophile elements to the core and leaves behind lithophile elements in the magma ocean (i.e., the mantle), establishing the compositions of both reservoirs. The relative depletion of siderophile elements in the mantle is evaluated by comparison between the compositions of the mantle and chondritic meteorites, which are considered to sample the undifferentiated building materials of planets (McDonough and Sun, 1995). Metal-silicate partitioning experiments of siderophile elements under high pressure and high temperature can then be used to match the observed depletions, and further constrain the pressure (P), temperature (T), composition and oxygen fugacity (fO_2) conditions of core formation (Li and Agee, 1996; Righter et al., 1997; Wade and Wood, 2005; Bouhifd and Jephcoat, 2011; Siebert et al., 2013; Badro et al., 2015; Fischer et al., 2015; Huang et al., 2020).

Like other 'geochemical twins' (e.g., Zr and Hf, Nb and Ta) vertically adjacent to each other in the periodic table, Mo and W share some important geo/cosmochemical properties. In particular, they are the only two moderately siderophile elements that are at the same time cosmochemically refractory. This makes them a useful monitor of core formation conditions, because they should accrete into the chondritic Earth in the same fashion as other refractory elements and then partition moderately into the core, maintaining their abundances resolvable in both mantle (not easily affected by later additions) and core after core formation. Additionally, the study of W is of broad interest due to the fact that the Hf-W isotope systematics provide important constraints on the timing of core formation (Kleine et al., 2002; Yin et al., 2002).

As two of the most intensively studied elements in terms of partitioning experiments, Mo and W have been found to vary their partitioning behavior dramatically as a function of P, T, silicate and metal compositions and fO_2, with a spread of measured partition coefficients over several orders of magnitude. Most importantly, they turn out to share many similarities in partitioning. For example, previous experimental studies have generally shown that

temperature, polymerization degree of silicate melt, carbon content in the metal have a positive effect (i.e., more siderophile), whereas pressure, fO_2, and sulfur/silicon content in the metal exert a negative influence on both Mo and W partitioning (i.e., more lithophile) (Walter and Thibault, 1995; Jana and Walker, 1997b,c; Righter et al., 2010; Siebert et al., 2011; Tuff et al., 2011; Wade et al., 2012; Shofner et al., 2014; Wood et al., 2014; Righter et al., 2016). A few studies have shown varying properties between Mo and W: Righter et al. (2010) and Siebert et al. (2011) reported opposite temperature dependence for Mo, Cottrell et al. (2009) found negative dependence on temperature and non-monotonic effect of pressure for W, and Jennings et al. (2021) observed negligible pressure influence on W partitioning. Apart from these disagreements as regards pressure and temperature, the partitioning of Mo and W further raises the question of delivery (especially the timing) of volatiles during Earth's accretion, such as sulfur and carbon. Stronger partitioning of W relative to Mo into the core, which contradicts the mantle abundances of Mo and W, requires S delivery to the Earth only during late stages of core formation (Wade et al., 2012; Wood et al., 2014). Recently, Jennings et al. (2021) found that the interactions between C and Mo (and W) would make both more siderophile, based on which their N-body accretion models favored a C-rich scenario in early accreting Earth, in order to reduce the mantle abundances of Mo and W to the observed values. Previous work on Mo and W has in general reached a reasonable level of agreement on the complex effect of P-T-composition-fO_2, yet the extrapolation to the P-T conditions relevant to a deep magma ocean is somewhat problematic. The aforementioned discrepancies on the effects and magnitudes of different variables on W and Mo partitioning, may be resolved by a much larger P-T range accessible with laser-heated diamond anvil cell (LHDAC) experiments.

The study of metal-silicate partitioning under extreme P-T conditions has been shown necessary to improve our understandings towards core formation. The so-called 'excess siderophile element problem' arises when one predicts their mantle concentrations based on partitioning experiments conducted at 1 bar (Ringwood, 1966). This apparent discrepancy between observation and prediction begins to converge at high pressures and temperatures, remarkably for Ni and Co (Li and Agee, 1996; Siebert et al., 2012), another two important moderately siderophile elements. In the case of both Mo and W, to date most metal-silicate partitioning experiments have a pressure limit of $\sim$25 GPa using piston-cylinder or multi-anvil press, even though much higher P–T conditions up to 75 GPa / 4350 K for core-mantle equilibration have

been recently modeled (Badro et al., 2014). Furthermore, the necessity of DAC experiments also resides in the possibility to probe the interactions of trace elements with oxygen in liquid metal. Unlike Si, S and C which have been widely studied under lower pressures, oxygen solubility in the metal is rather limited in large-volume press compared to LHDAC, because of the limited P-T conditions (Rubie et al., 2004; Asahara et al., 2007; Ricolleau et al., 2011; Siebert et al., 2012). The newly quantified influences of oxygen on siderophile (Siebert et al., 2013) and even lithophile (Badro et al., 2016; Blanchard et al., 2017; Chidester et al., 2017; Badro et al., 2018; Huang et al., 2020) elements have been shown to be dramatic, which warrants the study of Mo and W partitioning under higher P-T conditions in LHDAC. To the best of our knowledge, partitioning data under extreme P-T ($>$ 25 GPa) conditions is unavailable for Mo, and rare for W (Shofner et al., 2014). In this study, we aim to provide constraints on core formation by extending the P-T range of metal-silicate equilibration for Mo and W to 93 GPa and 4700 K, and by quantifying the effect of dissolved oxygen along with other light elements, under conditions comparable to a deep magma ocean.

2. Methods

2.1. Starting materials

The starting silicate glasses were synthesized using an aerodynamic levitation furnace at IPGP. High purity oxides (FeO, MgO, Al_2O_3, and SiO_2) and carbonate ($CaCO_3$) were ground and mixed in ethanol in an agate mortar, to produce a pyrolitic composition (McDonough and Sun, 1995) with low FeO content (4 wt%). The pyrolitic composition (Table S1) was used throughout to limit the effect of silicate melt composition on partitioning. W was added as ICP standard solution (in nitric acid) in one of the three different mixtures. The mixtures were then decarbonated at 950°C, and further transformed into glass beads in an Argon flux using the levitation furnace coupled with a 75 W CO_2 laser ($\lambda = 10.6$ μm). They were subsequently hand polished to $\sim$20 μm thick and machined into small disks suitable for DAC loading using a picosecond laser machining system at IPGP.

The metallic starting materials were either commercial reagent Fe-rich metal balls (91% Fe + 9% Si, or 96% Fe + 4% S) or synthetic Fe-Mo(-S). The latter alloy was synthesized in a piston-cylinder apparatus by equilibrating natural MORB (doped with Mo +/- S) with the commercial silicon-bearing iron alloy at 2 GPa and 1800°C for 2 minutes. Synthesized metal was then

crushed and finely ground to serve as starting metal for DAC experiments. The chemical homogeneity of both silicate glasses and metal was confirmed by microprobe (or EDS) results listed in Table S1.

2.2. Diamond anvil cell experiments

High pressure was generated using symmetric DACs. Re gaskets were pre-indented to 40-50 μm thick by diamond anvils with flat culet diameters of 200 μm or 300 μm. A hole of $\sim$100 μm or 150 μm in diameter was drilled in the gasket by a picosecond laser to form a sample chamber. Starting metals were loaded in between two layers of silicate disks which also served as thermal and chemical insulators during heating. Sample assembly was compressed to a pressure of interest and subsequently laser-heated from both sides using a fiber laser (λ = 1070 nm, 200 W) with a focused beam size of $\sim$20 μm in diameter. The laser power was ramped at first and then held for 30 to 60 seconds once reaching the target temperature, which was set well above the pyrolitic liquidus (e.g. 4700 K at 93 GPa) (Fiquet et al., 2010; Andrault et al., 2011), before quenching. Previous time series experiments under similar high P-T conditions have shown that the metal-silicate equilibrium can be attained in less than a few seconds (Walter and Thibault, 1995; Corgne et al., 2008) (details in Section 3.1). Temperature was measured continuously by fitting the visible portion of the black-body radiation (500–750 nm) from both sides of the heating spot to the Planck black-body function with an estimated uncertainty of $\pm$250 K (Benedetti and Loubeyre, 2004). Pressure was determined by diamond Raman spectroscopy before and after each experiment (Akahama and Kawamura, 2004), and corrected for thermal pressure (ΔP = 2.7 MPa/K) estimated from previous experiments following the same protocol with in situ X-ray diffraction measurements (Siebert et al., 2012).

2.3. Sample recovery and analysis

After quenching to ambient conditions, thin sections were extracted from the center of the laser-heated area using a Ga+ focused ion beam (FIB) instrument equipped with a field emission gun (Zeiss Auriga 40) at IPGP. Thin sections were removed from the gaskets by an in situ micromanipulator, and welded to TEM copper grids. A thin conductive layer of graphite ($\sim$10 nm thick) was deposited on the surface of the thin section for quantitative analysis. A backscattered electron image of the sample recovered from high pressure and temperature is shown in Fig. 1 as an example.

Chemical compositions of both metal and silicate phases were obtained by wavelength dispersive X-ray spectroscopy (WDS) using electron probe micro-analysis (EPMA) on a Cameca SX-five at Camparis, and reported in Table S2. An accelerating voltage of 25 kV and a beam current of 40 nA were used in all cases. Peak and background counting times were 15 s for major elements (Mg, Al, Ca, Fe and Si) in the silicate melts and for Fe in the quenched metals, and 60 s for minor and trace elements in both phases, including Si, O, Mg, Al and S in the metal. The detection limits were 100-400 ppm for most elements. Diopside (Ca and Mg), orthoclase (Al and Si), hematite (Fe and O), $BaSO_4$ (S) and pure Mo and W metals were employed as internal standards. Mo and W were analyzed using $L_{\alpha 1}$ line, whereas all the other elements using $K_{\alpha 1}$ line. For each metal and silicate phase, at least 5 spots were measured by microprobe to obtain the mean. To avoid secondary fluorescence from adjacent phases during analysis, samples were sectioned down to 3-4 μm thick with the same proportions of metal-to-silicate on both sides, and electron beam size less than 1μm was used to analyze the areas far enough (given the Z- and voltage-dependent interaction volume activated by the electron probe) from the metal-silicate phase boundary. Because quantitative chemical analysis using energy dispersive X-ray spectroscopy (EDS) coupled with FEG-FIB has shown an excellent agreement with EPMA results (Huang and Badro, 2018), we opted for EDS data for four of the samples (X5, X1, X4-1, X6-1, Table S2) whose silicate compositions were biased by the adjacent metal due to the large EPMA beam relative to the silicate. Accuracy of the EDS measurements is expected to be 1% based on the analytical calibrants.

Carbon diffusion from diamond anvils during heating was observed in the quenched metallic phase in some DAC experiments e.g., by Fischer et al. (2015). However, our previous superliquidus experiments following the same experimental procedure (Siebert et al., 2012, 2013) found carbon content below detection limit. We therefore infer carbon content in our samples to be insignificant, or below the detection limit of EPMA ($\sim$ 1wt%), based on the following additional observations: i) the molten silicate and metal are chemically isolated from the diamond anvils by a layer of untransformed solid glass (Fig. 1), and ii) quantitative EDS analyses show similar peak intensities of carbon in both metal and silicate melts, indicating that carbon contamination was likely introduced during analysis (e.g., by carbon coating or carbon tape), instead of during high-pressure experiments. However, even if C was below detection limit, its presence in the metal might still exert influence on

the partitioning of Mo and W, which needs to be addressed. Assuming the carbon content in all our metal liquids to be 1 wt%, the maximum amount estimated based on our previous discussion, we refit Eq. 11 (see Section 3), and compared the parameters with and without C in the metal (Table S5). As can be found in Table S5, the temperature (b) and pressure (c) terms in either case are indistinguishable from each other within uncertainties. This shows that the maximum 1 wt% C conceived in the metal has negligible effect on the partitioning of Mo and W.

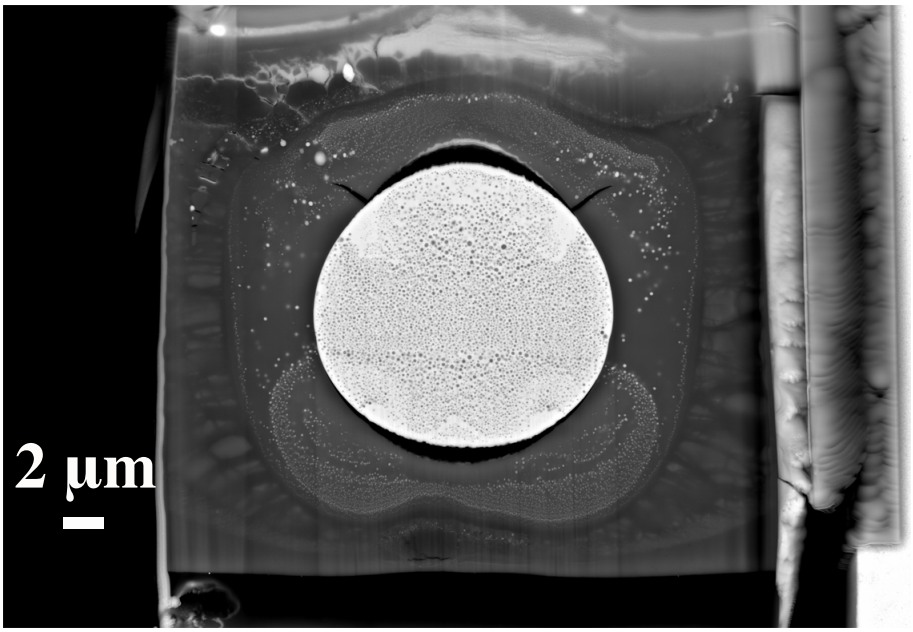

Figure 1: Backscattered electron image of a FIB section recovered from one of our diamond anvil cell experiments containing W at 48 GPa and 3670 K.

3. Results

Twelve superliquidus metal-silicate partitioning experiments in diamond anvil cells were performed at various P-T conditions and summarized in Table 1. Oxygen fugacity is evaluated relative to the iron-w$\ddot{u}$stite (IW) buffer:

$$fO_2(\Delta IW) = 2log\left(\frac{a_{FeO}^{sil}}{a_{Fe}^{met}}\right), \quad (1)$$

where a_{FeO}^{sil} and a_{Fe}^{met} are the activities of FeO and Fe in the silicate and metal, respectively, which are approximated as their mole fractions by assuming ideal behavior. Most of our experiments result in similar oxidized conditions (1 to 2 log units below the IW buffer) regardless of the reduced starting compositions with low-FeO silicates (Table S1), which is similar to previous studies using DACs (Siebert et al., 2012; Fischer et al., 2015; Badro et al., 2016; Huang and Badro, 2018). This may be explained by the increased partitioning of Si into the metal with increasing P-T resulting in metallic Fe being oxidized, and of FeO from solid to liquid silicate due to its incompatibility (cf. Siebert et al. (2012)).

The typical morphology of a recovered sample consists of a spherical metallic blob embedded in a silicate melt, as shown in Fig. 1. Quench textures were formed by rapid exsolutions of Si-O-rich (in the metal) and Fe-rich blobs (in the silicate) (both < 200 nm) during the quench. These features were observed in all our experiments, and shared by previous partitioning studies using LHDAC (Siebert et al., 2012; Fischer et al., 2015; Badro et al., 2016; Huang and Badro, 2018). Although it seemingly exhibits zonation in both phases, point analysis at the length scale of 1-2 μm (estimated from the X-ray excitation volume for metal and silicate phases) and larger window analysis (raster-scanned electron beam, whenever possible) show chemical homogeneity within each phase over the entire thin section (Table S2).

Table 1: Runs summary for the diamond anvil cell experiments.

Exp. No.	X5	X1	X4-1	X6-1	X4-J	X6-J	X4-2	X17	X7	X6-2	X9	X3
Pressure (GPa)	57(6)	39(4)	70(7)	93(9)	54(5)	41(4)	48(5)	60(6)	71(7)	48(5)	58(6)	71(7)
Temperature (K)	3950(200)	3020(150)	4190(210)	4670(250)	3600(180)	3100(160)	3670(180)	4070(200)	4250(220)	3700(190)	4050(200)	4290(220)
fO_2 (ΔIW) [a]	-2.6	-1.4	-1.7	-3.5	-1.4	-1.7	-1.3	-1.3	-1.3	-1.3	-1.5	-1.2
Starting Metal	Fe-Mo alloy	Fe-Mo alloy	Fe-Mo alloy	Fe-Mo alloy	Fe-Mo-S alloy	Fe-Mo-S alloy	Fe-Si alloy	Fe-Si alloy	Fe-Si alloy	Fe-S alloy	Fe-S alloy	Fe-S alloy
Starting Silicate [b]	PYR4-1	PYR4-1	PYR4-1	PYR4-1	PYR-J	PYR-J	PYR-W	PYR-W	PYR-W	PYR-W	PYR-W	PYR-W
D_{Mo}	22(10)	25(5)	25(7)	58(14)	20(6)	31(9)						
D_W							26(5)	16(4)	32(8)	29(5)	12(2)	9(1)

Note: (a) Oxygen fugacity relative to the iron-wüstite buffer is approximated as $fO_2(\Delta IW) = 2log_{10}(x_{FeO}/x_{Fe})$, assuming ideal mixing. (b) PYR denotes pyrolite, which were synthesized with 4wt% FeO, see Table S1.

3.1. Attainment of equilibrium

The time needed to reach chemical equilibrium for a given element between two phases is governed by the diffusion rate of that element. The characteristic length of diffusion λ is calculated by diffusion coefficient D and time t using

$$\lambda = 2\sqrt{D \cdot t}. \tag{2}$$

It has been proposed that diffusion coefficients for principal elements in silicate melt are 10^{-11} to 10^{-9} m^2/s from 1800 to 2800 K, 15 to 25 GPa by

Walker and Agee (1989) and 10^{-10} to 10^{-9} m^2/s at 4000 K and 136 GPa by Karki et al. (2010). On the other hand, recent ab initio calculations showed that self-diffusion coefficients for Fe, Si and O in liquid metal are on the orders of 10^{-7}-10^{-8} m^2/s under core pressures with temperatures higher than 3800 K (Pozzo et al., 2013; Huang et al., 2019). Moreover, time series experiments demonstrated that partitioning equilibrium was achieved within 5 s at 5 GPa and 2300 K for Ni and less than 20 s at 2273 K and 3.6 GPa for a series of elements with a typical sample size of a few millimeters (Corgne et al., 2008; Thibault and Walter, 1995). Given the above range of diffusivity, the extremely high temperatures (from 3000 to 4700 K) and small samples (a few micrometers), the equilibrium should be readily attained within the typical duration of ∼60 s in our experimental run. The attainment of equilibrium between molten silicate and liquid metal can also find supports from (1) the compositional homogeneity, as indicated by the small standard deviations, observed in the quenched phases in Table S2, and (2) consistency within the same thermodynamic model between DAC data and low-P data obtained from piston-cylinder or multi-anvil press, as will be discussed in the following text.

3.2. Equilibrium constant

The partitioning of an element M between molten metal and silicate takes place according to an exchange reaction:

$$MO_{n/2} + \frac{n}{2}Fe = \frac{n}{2}FeO + M \tag{3}$$

that combines two redox reactions:

$$MO_{n/2} = \frac{n}{4}O_2 + M \tag{4}$$

and

$$\frac{n}{2}Fe + \frac{n}{4}O_2 = \frac{n}{2}FeO, \tag{5}$$

where n is the valence of the cation M in the silicate melt. The partition coefficient of element M is calculated using molar fractions (x) of M in the relevant phase by $D_M = \frac{x_M}{x_{MO_{n/2}}}$. D is a function of P, T, composition and oxygen fugacity. The exchange coefficient, $K_D = D_M/D_{Fe}^{n/2}$, can be considered partition coefficient D_M corrected for oxygen fugacity which is conveniently expressed as D_{Fe}. The equilibrium constant K of reaction 3 can

then be defined in terms of K_D and activity coefficients (γ) in the silicate and metallic phases by

$$logK = logK_D + log(\frac{\gamma_M}{\gamma_{Fe}^{n/2}})^{metal} + log(\frac{\gamma_{FeO}^{n/2}}{\gamma_{MO_{n/2}}})^{silicate}. \quad (6)$$

The valence (n) of Mo and W has been reported to change with redox condition, while being insensitive to pressure and temperature in the previously investigated P-T range (Wade et al., 2012; Righter et al., 2016). Following previous studies, where Mo was found in tetravalent state (Righter et al., 2016) and W in 6+ (Wade et al., 2012) at fO_2 lower than 1 log unit below the IW buffer, we fixed the valence of Mo and W to 4+ and 6+ respectively, given reducing conditions (IW-1 to IW-3) observed in our experiments. The ratio of oxide activity coefficients in silicate melt (last term in Eq. 6) may be assumed independent of melt composition for low valence cations (e.g., Ni^{2+} and Co^{2+}) (O'Neill and Eggins, 2002; O'Neill and Berry, 2006), however, for high valence cations it may vary by a much higher degree. We thus introduced an empirical parameter to model the effect of silicate composition, particularly the degree of polymerization, which will be detailed in 3.3.2.

The activity coefficients in the metal are significantly influenced by the light elements dissolved in liquid iron, such as Si, O, S and C (Jana and Walker, 1997a,c; Tuff et al., 2011; Wood et al., 2014). To model the interactions in the metal and to correct the effects of the alloy composition on partitioning, we used the interaction parameter (ϵ) approach proposed by Ma (2001), to calculate the activity coefficients in the Fe-rich alloy. This has become standard practice in regard to metal-silicate partitioning (Wade and Wood, 2005; Corgne et al., 2009; Ricolleau et al., 2011; Siebert et al., 2013; Huang and Badro, 2018). Following this method, the activity coefficients of the solvent (Fe) and $N-1$ solutes (i) for N components metallic solutions

can be expressed as

$$
\begin{aligned}
ln\gamma_{Fe} = & \sum_{i=1}^{N-1} \epsilon_i^i (x_i + ln(1-x_i)) \\
& - \sum_{j=1}^{N-2} \sum_{k=j+1}^{N-1} \epsilon_j^k x_j x_k \left(1 + \frac{ln(1-x_j)}{x_j} + \frac{ln(1-x_k)}{x_k}\right) \\
& + \sum_{i=1}^{N-1} \sum_{k=1(k\neq i)}^{N-1} \epsilon_i^k x_i x_k \left(1 + \frac{ln(1-x_k)}{x_k} - \frac{1}{1-x_i}\right) \\
& + \frac{1}{2} \sum_{j=1}^{N-2} \sum_{k=j+1}^{N-1} \epsilon_j^k x_j^2 x_k^2 \left(\frac{1}{1-x_j} + \frac{1}{1-x_k} - 1\right) \\
& - \sum_{i=1}^{N-1} \sum_{k=1(k\neq i)}^{N-1} \epsilon_i^k x_i^2 x_k^2 \left(\frac{1}{1-x_i} + \frac{1}{1-x_k} + \frac{x_i}{2(1-x_i)^2} - 1\right),
\end{aligned}
\tag{7}
$$

and

$$
\begin{aligned}
ln\gamma_i = & ln\gamma_{Fe} + ln\gamma_i^0 - \epsilon_i^i ln(1-x_i) \\
& - \sum_{j=1(j\neq i)}^{N-1} \epsilon_i^j x_j \left(1 + \frac{ln(1-x_j)}{x_j} - \frac{1}{1-x_i}\right) \\
& + \sum_{j=1(j\neq i)}^{N-1} \epsilon_i^j x_j^2 x_i \left(\frac{1}{1-x_i} + \frac{1}{1-x_j} + \frac{x_i}{2(1-x_i)^2} - 1\right),
\end{aligned}
\tag{8}
$$

where γ_i^0 is the activity coefficient of solute i in liquid iron at infinite dilution, ϵ_i^j the interaction parameter of element j on element i and x_i the mole fraction of element i in the metal. Interactions between minor/trace metals (Mo and W) are not considered, since their influence on each other is supposed to be negligible due to the low abundances. We fit ϵ_i^j between light-element species (Si, O, C and S) and minor/trace metals, at the reference temperature 1873 K (T^0), together with γ_i^0 taken from Steelmaking Data Sourcebook (JSPSNCS, 1988). ϵ_i^j and γ_i^0 are then extrapolated to run temperatures according to

$$
ln\gamma_i^0(T) = \frac{T^0}{T} ln\gamma_i^0(T^0), \tag{9}
$$

$$
\epsilon_i^j(T) = \frac{T^0}{T} \epsilon_i^j(T^0). \tag{10}
$$

3.3. Partitioning of Mo and W

In order to parameterize the effects of thermodynamic parameters on the partitioning of Mo and W during core formation, and to obtain better statistics for the parameterization, we compiled partitioning data from the literature on Mo (Hillgren et al., 1996; Jana and Walker, 1997a,b; Righter et al., 2010; Siebert et al., 2011; Tuff et al., 2011; Wade et al., 2012; Wood et al., 2014; Jennings et al., 2021) and W (Hillgren et al., 1996; Jana and Walker, 1997a,b; Righter and Shearer, 2003; Cottrell et al., 2009; Righter et al., 2010; Tuff et al., 2011; Siebert et al., 2011, 2012; Wade et al., 2012; Wood et al., 2014; Jennings et al., 2021). These data are plotted in Figs. 2-3, together with our data. It is notable that there is a lack of partitioning data for both Mo and W when pressure exceeds 25 GPa. By means of multivariate least-squares linear regression, the calculated nominal equilibrium constant ($logK = logK_D + log\frac{\gamma_M}{\gamma_{Fe}^{n/2}}$, reported in Tables S3-S4) using the interaction parameter approach were fitted to the thermodynamic model described by

$$logK = a + \frac{b}{T} + c\frac{P}{T} + d \cdot (nbo/t - 2.7)\,, \tag{11}$$

where a is the entropy ($\Delta S^0/2.303R$), b the enthalpy ($-\Delta H^0/2.303R$), and c the volume ($-\Delta V^0/2.303R$) change of reaction 3 (superscript 0 denotes the standard state and R is the ideal gas constant). As discussed earlier, to account for the compositional effect of silicate melt (i.e., activity ratio, last term in Eq. 6) on partitioning of highly charged Mo (4+) and W (6+), we introduced an empirical parameter nbo/t (Mysen, 1983), the molar ratio of non-bridging oxygens (nbo) per tetrahedrally coordinated cations (t), which was corrected to a pyrolitic composition whose nbo/t equals 2.7. A stepwise regression was performed according to the following steps. Firstly, all coefficients, namely a, b, c, d, and interaction parameters (ϵ_i^j) between light elements (Si, O, C, and S) and the elements of interest (Mo and W), were fitted to the simultaneous equations (Eqs. 6-11) (step 1). After the statistically insignificant interaction parameters (see details in Section 3.3.3) were set to 0, the remaining coefficients were fitted again (step 2). The resulting interaction parameters from step 2 were then fixed (i.e., the ϵ_i^j values listed in Table 2), and a, b, c, and d were regressed a third time (step 3). The fitting results obtained in step 3 are consistent with the simultaneous fit of all the coefficients in step 1, whereas the uncertainties from the final regression are more relevant statistically. The parameterizations using Eq.

11 will enable us to evaluate individual effects of pressure, temperature and silicate composition on the partitioning of Mo and W, as follows.

Table 2: Thermodynamic parameters of the metal-silicate partitioning of Mo and W.

Element (i)	a	b (K)	c (K/GPa)	d	ϵ_i^O	ϵ_i^{Si}	ϵ_i^C	ϵ_i^S	ϵ_i^i	$ln\gamma_i^0$	N	R^2
Mo	4.1(6)	-5563(1139)	-215(21)	-0.60(7)	-17(9)	29(1)	-8(1)	0	3.955	0	138	0.6
W	1.8(3)	-6942(596)	-84(11)	-0.69(4)	-15(6)	0	-9(1)	8(2)	0	0	259	0.6
O						-7	-20	-17.1	-1			
Si							3.6	9	12.4			
C								4.9	12.8			
S									-5.7			

Notes: Parameters of Eq. 11 for Mo and W partitioning: a, b and c represent the entropy, enthalpy and volume change of the reaction, and d the effect of silicate melt. Values in parenthesis are standard errors (1 σ) obtained from the least-squares regressions. ϵ_i^j is the interaction parameter of element j on element i and γ_i^0 the activity coefficient of solute i at infinite dilution in liquid iron; interaction parameters are calculated from this study, except for those between light species (Si, O, C and S) which are from JSPSNCS (1988) (see Part II: Tables 2.1 and 2.3 therein). Self-interaction parameters ϵ_i^i and γ_i^0 are also taken from JSPSNCS (1988) (see Part II: Tables 1 and 2.1 therein). Interaction parameters and activity coefficients are reported at 1873 K (see details in section 3.2). N is the number of data used in each regression, and R^2 the coefficient of determination of the fitted model.

3.3.1. Pressure and temperature effect

Of the data compiled for Mo and W, most were obtained at experimental pressures well below 25 GPa (Fig. 2, blue dots). Our twelve experiments performed at higher pressures thus probe the partitioning behavior at the conditions of deep core formation. Under these extreme environments, we find that Mo and W more strongly partition into metallic liquid with increasing temperature (higher log K), while less so with pressure (lower log K), as can be found in Fig. 2.

The negative pressure effect (c = -84±11 K/GPa, Table 2) on W partitioning is indistinguishable from previous multi-anvil results by Siebert et al. (2011) (c = -55±35 K/GPa) and Wade et al. (2012) (c = -77 K/GPa), though to a more evident extent; the similar but more profound pressure effect on Mo partitioning (c = -215±21 K/GPa) is consistent with Wade et al. (2012) (c = -167 K/GPa). Recently, Jennings et al. (2021) found negligible and weak pressure terms on W and Mo, respectively. The reason is that their expressions may lose accuracy at higher pressures due to the limited pressure range, as provided in their own note of caution.

Similarly, for both Mo and W, temperature increases the affinity of these elements for the metallic phase ($b < 0$ K). The influence of temperature on partitioning was debated for both Mo (Siebert et al., 2011; Wade et al., 2012) and W (Cottrell et al., 2009; Wade et al., 2012). The increasing siderophility of W with temperature is well defined here, given the wide temperature range (from 1773 to 4700 K) covered by combining present and previous data: temperature dependence for Mo and W can be clearly seen if one

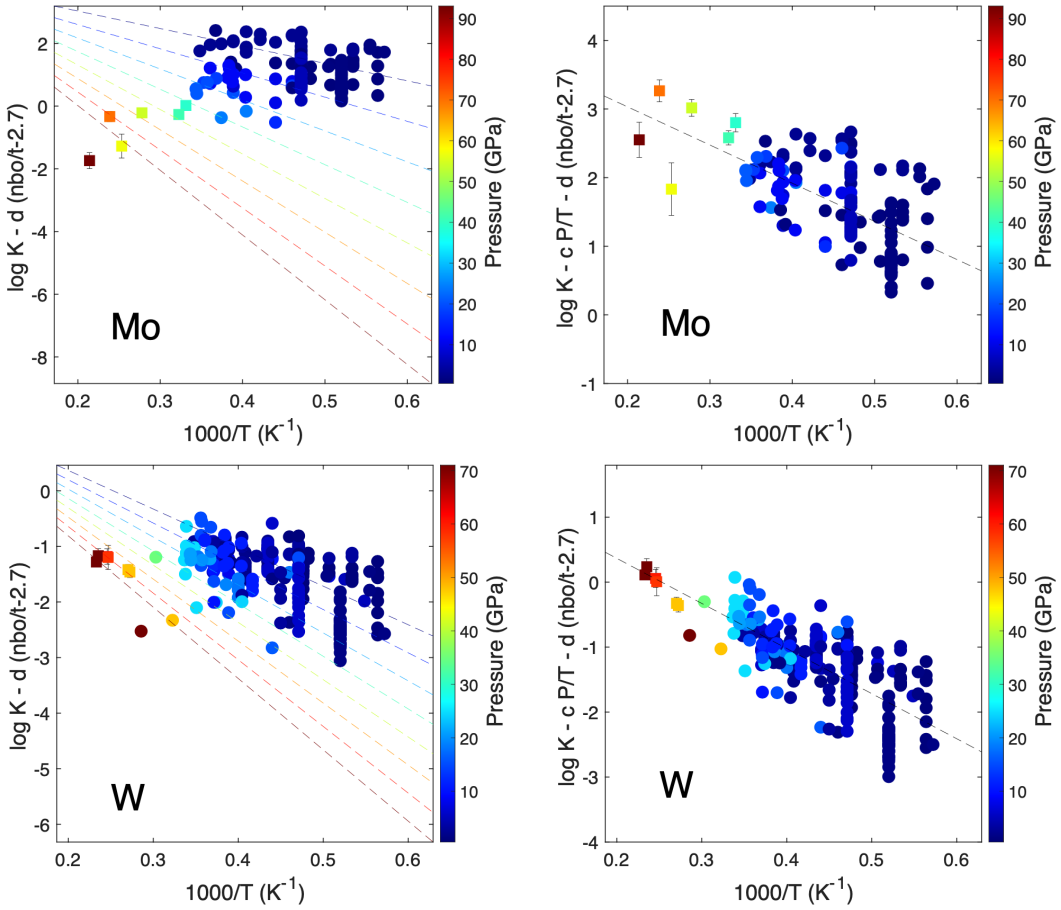

Figure 2: Pressure and temperature effect on the partitioning of Mo and W. Equilibrium constants (log K) for Mo and W are plotted as a function of reciprocal temperature (1000/T). Pressure is reported in symbol color. Experimental data for Mo are taken from Hillgren et al. (1996); Jana and Walker (1997a,b); Righter et al. (2010); Siebert et al. (2011); Tuff et al. (2011); Wade et al. (2012); Wood et al. (2014); Jennings et al. (2021) and this study (squares). W data are taken from Hillgren et al. (1996); Jana and Walker (1997a,b); Righter and Shearer (2003); Cottrell et al. (2009); Righter et al. (2010); Tuff et al. (2011); Siebert et al. (2011, 2012); Wade et al. (2012); Wood et al. (2014); Jennings et al. (2021) and this study (squares). Error bars (shown where larger than symbols, for this study) were propagated from the analytical uncertainties in Table 2. In the left panels, equilibrium constants are corrected for silicate melt compositions (log K - d (nbo/t - 2.7), in order to show the P-T dependence; the dashed lines are isobars (color-coded as well) obtained from least-squares linear regressions (Eq. 11) to the data, showing temperature dependence at a given pressure, or pressure dependence at a fixed temperature. In the right panels, equilibrium constants are corrected for both pressure and silicate melt compositions (log K - c P/T - d (nbo/t - 2.7), the black dashed lines), to solely illustrate partitioning as a function of reciprocal temperature.

eliminates the effects of pressure and silicate composition by correcting for the pressure and compositional (c and d) terms from the same dataset, as shown in Fig. 2 (right panels).

Since pressure and temperature are correlated parameters in the regression, it would be useful to compare their effects together. Table S6 lists the fitted parameters for b and c terms from present and previous studies. For Mo, the combined P-T effects (c and b terms, Table S6) generally agree with the recent work by Jennings et al. (2021), while differing from the extents to which P and T affect the partitioning. The P-T effects on W partitioning, on the other hand, are consistent with most previous results as regards the signs (Siebert et al., 2011; Shofner et al., 2014), and within uncertainties are identical to the results found in Wade et al. (2012) (Table S6).

3.3.2. Dependence on silicate melt composition

It has been shown that silicate melt composition, particularly the degree of polymerization which is conveniently parameterized as a function of nbo/t, can significantly affect the partitioning behavior between metal and silicate (Walter and Thibault, 1995; Jana and Walker, 1997b; O'Neill and Eggins, 2002; Chabot and Agee, 2003), especially for high valence state cations like Mo and W. Since the coordination environment in silicate changes from tetrahedra to octahedra at upper mantle conditions (10 to 20 GPa), the nbo/t calculation is no longer applicable to our higher P data ($>$ 40 GPa). We therefore only calculated and fitted the nbo/t values for previous data less than 25 GPa, and kept our nbo/t constant at the pyrolitic value of 2.7 in all the regressions. The corrected (for pressure and temperature) equilibrium constant K ($<$25 GPa) in log units is plotted as a function of nbo/t in Figure 3.

In agreement with previous observations (Walter and Thibault, 1995; Jana and Walker, 1997b; Cottrell et al., 2009; Siebert et al., 2011), Mo and W become more lithophile in less polymerized melt (higher nbo/t). The reason, since they are not considered tetrahedral cations, may be that highly charged Mo and W cations require more non-bridging oxygen atoms in order to be stably incorporated in the silicate network.

3.3.3. Influence of light elements in liquid metal

The effect of light species on the partitioning behavior of Mo and/or W has been extensively characterized, to name only a few recent examples, for carbon (Cottrell et al., 2009; Siebert et al., 2011; Jennings et al., 2021), sulfur

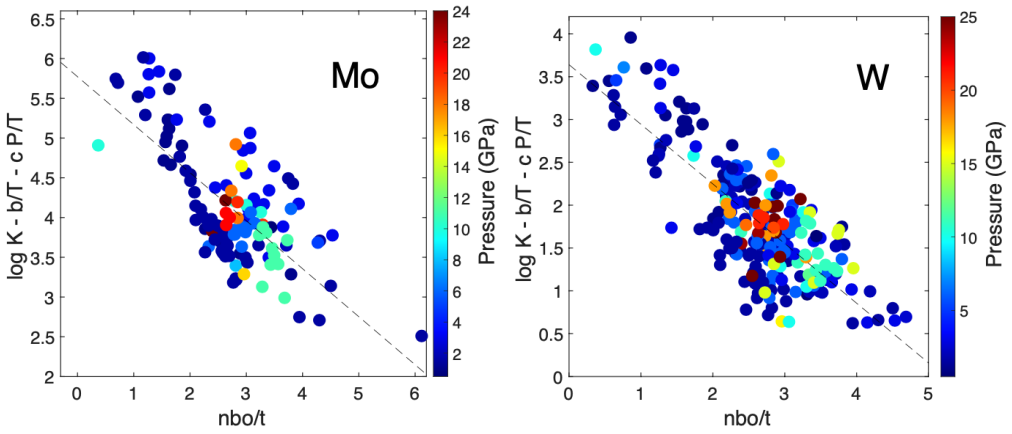

Figure 3: Equilibrium constants (log K) for experiments conducted under 25 GPa as a function of nbo/t for Mo and W. Following the same rationale as in Fig. 2, P and T effect (c and b terms in Eq. 11) are removed, i.e., log K -b/T -c P/T (solid dots), to reveal the effect of nbo/t. The partitioning of Mo and W is both strongly influenced by the degree of polymerization of silicate melt: both elements become more siderophile with decreasing nbo/t, consistent with previous results from Walter and Thibault (1995); Jana and Walker (1997b); Cottrell et al. (2009); Siebert et al. (2011).

(Wade et al., 2012) and silicon (Tuff et al., 2011). Recently, it becomes possible to quantity that of oxygen, when partitioning experiments under much higher P-T conditions are available in LHDACs: because such conditions greatly promote the partitioning of FeO into liquid metal. This can be seen by the fact that, while the starting metal contained neither oxygen nor any lithophile elements (see Table S1), oxygen, magnesium and aluminum were observed along with siderophile elements in recovered metal (Table S2).

The minor amounts of oxygen in our metals, between 3 to 8 wt%, allow for characterization of its interactions with Mo and W. Using the activity model described above and combining Eqs. 6-11, we have modeled the effect of oxygen, along with Si, C and S, by fitting the interaction parameter ϵ. The fitting results are listed in Table 2. We find the absolute values of ϵ^O_{Mo}(=-17) and ϵ^O_W(=-15) to be significantly larger than those tabulated in JSPSNCS (1988), where ϵ^O_{Mo}=1.3 and ϵ^O_W=4.1. This means that oxygen dissolved in liquid iron has more pronounced influence on the partitioning of Mo and W than previously thought. Meanwhile, the negative signs of ϵ^O_i indicate that oxygen increases the siderophility of both elements.

Si is another important light element in Earth's core, and is known to

interact strongly with Mo, as the value of 933 for ϵ_{Mo}^{Si} listed in JSPSNCS (1988) indicates. Our experiments show a wide range of Si contents in the metal, 1.5-12.8 wt%; when augmented by all available data (Table S3), we find ϵ_{Mo}^{Si} of 29(1), a value much lower than 933 but close to the recent value of 22(5) found by Tuff et al. (2011). In contrast to Tuff et al. (2011) who reported ϵ_{W}^{Si} of 18.3, we find it statistically insignificant (ϵ_{W}^{Si}=0). This is because the strong correlation between ϵ_{W}^{Si} and ϵ_{W}^{O} (Pearson correlation coefficient r=0.84), revealed by our higher pressure results, determines that only ϵ_{W}^{O} remains significant in the linear regression. Although carbon concentration is assumed negligible in our metal (see Methods), we have fit ϵ_{i}^{C} based on a large C-containing dataset with up to 38 mol% C in the metal, which yields ϵ_{Mo}^{C}=-8(1), ϵ_{W}^{C}=-9(1), consistent with the values of -6 and -3 for Mo and W by JSPSNCS (1988), and identical to -7.0(3) and -7.4(6) for Mo and W by Jennings et al. (2021) within uncertainties.

S was intentionally added to nearly half of our experiments (Table 1), which ended up with 3-8 wt% in the metals. Combining with 57 and 55 S-containing data for Mo and W respectively from the literature (Table S3-S4), we find ϵ_{Mo}^{S} insignificant in the thermodynamic regression, slightly differing from the value of 2.27 Wood et al. (2014), but in line with ϵ_{Mo}^{S}(=0.3) close to zero in JSPSNCS (1988). Unlike Mo, the S-W interaction is much more remarkable, and our value of 8(2) for ϵ_{W}^{S} is in good agreement with 5.94 and 6.47 found in JSPSNCS (1988) and Wood et al. (2014).

4. Discussion: applications to core formation

Equations 6 and 11 can be combined and rearranged as follows:

$$logD_M = a + \frac{b}{T} + c\frac{P}{T} - \frac{n}{2}log\frac{x_{FeO}}{x_{Fe}} - log\frac{\gamma_M}{\gamma_{Fe}^{n/2}}, \tag{12}$$

where the ratio of activity coefficients in silicate melt in Eq. 6 has been approximated by fitting the nbo/t in Eq. 11, which is canceled by assuming a pyrolitic silicate melt (nbo/t = 2.7) in the magma ocean. Using Eq. 12, in principle, the elemental distribution between metal and silicate can be predicted at a given P, T, fO_2 and metal composition.

Since the Earth's core formation is thought to take place in a continuous fashion during its accretion, we model a multistage core formation process where the Earth is accreted in 100 steps (Fig. 4). At each step, the metal

from the accreted material fully equilibrates with the entire magma ocean at its base, whose pressure and temperature are calculated as a function of total accreted mass and magma ocean depth and by using the mantle liquidus in Andrault et al. (2011). In order to reach the observed Ni and Co abundances in the mantle, the final equilibrium pressure and temperature at the end of Earth's accretion is determined to be 50 GPa and 3280 K (Fig. 4a), consistent with recent estimates from single-stage (Siebert et al., 2012; Fischer et al., 2015) and multi-stage core formation models (Badro et al., 2015; Huang et al., 2020), as well as N-body accretion simulations (Rubie et al., 2015). The FeO content of the magma ocean (mantle) is imposed to follow a given redox path. The ratio of activity coefficients in the metallic phase is calculated self-consistently by predicting the amount of Si and O dissolved in liquid Fe following the Si-O model in (Siebert et al., 2013). Recent N-body simulations (Jennings et al., 2021) took account of i) partial equilibrium between the impacting cores and Earth's mantle, and ii) a range of composition as regards redox state in accreting bodies, such that it may explain their overabundant W in the mantle. However, our accretion model does not include these two aspects, because we consider that i) the nature of impacting bodies might not be well constrained, and ii) full equilibration hypothesis works well here and hence does not require partial equilibrium, which would add more free parameters than already desired in this study.

Based on the results of our regression (Table 2) for Mo and W, their elemental distribution between metal and silicate is calculated at each accretion step and integrated until the core is fully formed. We firstly find that a growing Earth, taking only Si and O as major light components in its core (dashed lines in Fig. 4b), would be too much enriched in Mo relative to W in its mantle (low D_{Mo} and high D_W). This would result in a retreat to the old dilemma where W is found too siderophile compared to Mo by the end of accretion (Wade et al., 2012; Wood et al., 2014), which leads to an overestimated Mo/W ratio in Earth's mantle (dashed lines in Fig. 4, lower panels). Although, in contrary to the above-mentioned studies, Mo remains more siderophile than W during most of the accretion (during which Mo/W ratio is faithfully reproduced too, Fig. 4f); it only becomes less so (mainly affected by pressure, whose effect is now better constrained) by the end of core formation where pressures are higher.

Fig. 4 shows results of core formation at constant fO_2 with FeO content in the mantle equal to that of present-day Earth (Fig. 4c). Keeping a constant fO_2 is a simple but effective way to examine the effects of other

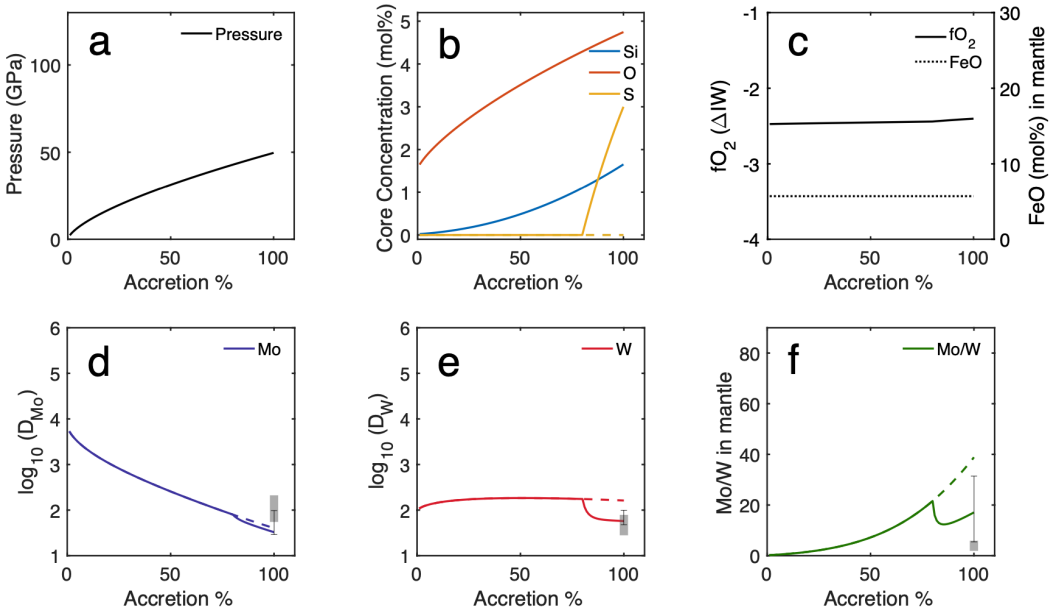

Figure 4: Results of Earth's core formation modeling as a function of accreted Earth's mass (%) with (solid lines) and without (dashed lines) S addition during the last 20% accretion. Upper panel (from left to right): the evolution of (a) pressure for metal-silicate equilibration, (b) concentrations of light elements (Si, O and S) in the core (mol%), and (c) bulk fO_2 (relative to IW buffer, solid line) between Earth's core and mantle as well as FeO content in the mantle (dotted line). Lower panel (from left to right): Core-mantle partition coefficients (in log unit) of (d) Mo (blue) and (e) W (red), and (f) Mo/W ratio (green) in the mantle. Dashed lines: S-free throughout the accretion. Solid lines: S is added only during the last 20% of the accretion. Grey shaded rectangles represent Earth targets to match from McDonough and Sun (1995) and Palme and O'Neill (2014). Error bars are propagated from the uncertainties on the thermodynamic parameters in Table 2 using Monte-Carlo simulation. The observables, D_{Mo}, D_W and Mo/W ratio in the mantle, are simultaneously matched only when S is accreted during late accretion.

variables (P, T and composition); alternatively, evolving the Earth under reducing or oxidizing conditions may offer a solution. However, after extensive experimenting, we find that modifications to the redox path, by building the Earth from either oxidized or reduced materials, do not alleviate the Mo/W ratio problem. Although a previous study found the same (Wade et al., 2012), it seems counter-intuitive given the valence difference between W (6+) and Mo (4+). The reason may be that the partitioning between core and mantle is not entirely controlled by fO_2, but determined by the interplay of P, T, fO_2, and composition. Since pressure and temperature conditions of Earth's core formation are predetermined by Ni and Co partitioning (Li and Agee, 1996; Siebert et al., 2012; Fischer et al., 2015; Huang and Badro, 2018) and mantle liquidus, we are inevitably led to look into the effect of light species in the core.

The partitioning of Si and O is calculated using the Si-O solution model as in Siebert et al. (2013) (Fig. 4b), and their influence on the behavior of Mo and W has been incorporated in our model through the calculations of activities γ_{Mo} and γ_W. On the other hand, interaction parameters in Table 2 indicate a strong negative interaction between S and W, ϵ_W^S=8, in stark contrast to Mo, which should be little affected by S content in the metal (ϵ_{Mo}^S=0). The solution seems to reside in S.

Based on cosmo/geochemical observations, S content of Earth's core is estimated ∼2 wt% (Mcdonough, 2003). We thus devised a model where the delivery of 2% S begins at different stages of the accretion. As can be seen in Fig. 5, if S is accreted throughout the process (x=0, i.e., homogeneous accretion), the effect of S would be minimal and W would be overly siderophile. However, when S is to be enriched in the metal towards the end, particularly after 80% of the accretion, we find that D_W drops significantly, while D_{Mo} remains almost unaltered, such that all three observables being reproduced. One of our best fits where 2 wt% (3 mol%) S is added during the last 20% accretion is shown in Fig. 4 in solid lines. Interestingly, despite the updated effects of pressure, temperature and metal composition resolved from our high pressure data combined with all available literature data, we coincide in the late addition of S with previous work at lower pressures (Wade et al., 2012; Wood et al., 2014). Apart from this consistency from lower to higher pressures for Mo and W partitioning, the late addition of sulfur finds supports in their mantle abundances estimated from the partitioning of S (Suer et al., 2017), Zn (Mahan et al., 2018), and moderately volatile and siderophile elements (Kubik et al., 2021), as well as dynamical simulations

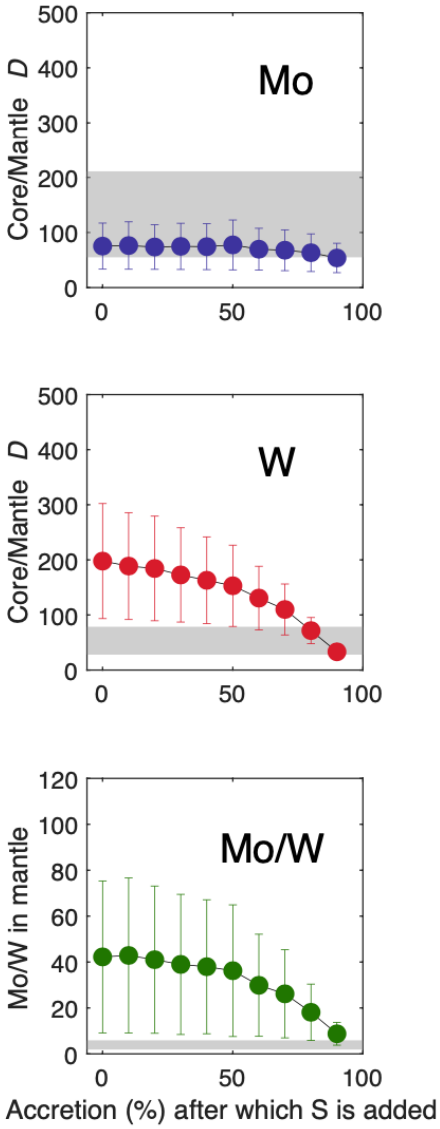

Figure 5: Bulk partition coefficients for Mo and W between Earth's core and mantle, and Mo/W ratio in the mantle, versus timing of S addition to the core. Each point corresponds to an endpoint of the same multistage core formation model as in Fig. 4. The uncertainties are the intervals of partition coefficient calculated by Monte-Carlo simulation. Horizontal grey patches represent Earth targets from McDonough and Sun (1995) and Palme and O'Neill (2014). The addition of 2 wt% S towards the end of accretion greatly decreases D_W, resulting in the correct reproduction of the observed Mo/W ratio.

(Raymond et al., 2009) and recent volatile data for chondrites (Braukmüller et al., 2019) that favor a late delivery of volatile-rich materials to the Earth. Moreover, our findings are compatible with heterogeneous accretion models that could explain various isotopic signatures of the Earth and other bodies alike (Albarède, 2009; Schönbächler et al., 2010).

The influence of C on Mo and W partitioning is also tested. However, due to the nearly equivalent interactions between C-W and C-Mo (ϵ_i^C in Table 2), the sequestration of small amount of C, $\sim$1 wt% in the core (Wood et al., 2013), equally adjusts D_W and D_{Mo}. Carbon therefore does not offer an effective solution. As regards the light-element candidates in the core, to this study it would seem likely a mixture of Si, O, S and probably C (which we are unable to discriminate).

5. Conclusions

Superliquidus metal-silicate partitioning experiments have been performed on Mo and W in twelve diamond anvil cells under high P-T conditions up to 93 GPa and 4700 K. When combined with available literature data, both Mo and W are found to be less siderophile with increasing pressure, with Mo being more significantly influenced. In contrast, temperature similarly promotes the partitioning of Mo and W into the metal. At pressures lower than 25 GPa, the non-bridging oxygen/tetrahedral cation (nbo/t) adequately models the effect of silicate melt composition on highly charged Mo and W cations. Oxygen dissolved in liquid metal interacts more strongly with Mo and W than previously considered. W partitioning is notably more sensitive to S content of the metallic liquid than Mo.

The application of our results to a multi-stage core formation model shows that homogeneous accretion of the Earth produces the observed Mo concentration in its mantle, but underestimates W abundance and thus ends up with an overestimation of the Mo/W ratio. The late addition of 2 wt% S to the core after 80 % of Earth's accretion reconciles the 3-observable problem by making W less siderophile. Parameterizations for Mo, and especially W, can be used in the future to model physical conditions as well as timing of core formation.

Acknowledgements

We thank Nicolas Wehr for help with high-pressure experiments; Stephan Borensztajn for assistance with focused ion beam samples preparation; Michel

Fialin and Nicolas Rividi for help with EPMA analysis. J.B. acknowledges funding from the European Research Council under the European Community's Seventh Framework Programme (FP7/2007-2013) / ERC Grant 207467. J.S. and D.H. acknowledge support from the French National Research Agency (ANR project VolTerre, Grant ANR-14-CE33-0017-01). We acknowledge the financial support of the UnivEarthS Labex program at Sorbonne Paris Cité (ANR-10-LABX-0023 and ANR-11-IDEX-0005-02). Parts of this work were supported by IPGP multidisciplinary program PARI (Plateforme d'analyse haute résolution), and by Paris–IdF region SESAME (Soutien aux Equipes Scientifiques pour l'Acquisition de Moyens Expérimentaux) Grant 12015908.

References

Akahama, Y., Kawamura, H., 2004. High-pressure Raman spectroscopy of diamond anvils to 250 GPa: Method for pressure determination in the multimegabar pressure range. Journal of Applied Physics 96, 3748–3751.

Albarède, F., 2009. Volatile accretion history of the terrestrial planets and dynamic implications. Nature 461, 1227–1233.

Andrault, D., Bolfan-Casanova, N., Nigro, G.L., Bouhifd, M.A., Garbarino, G., Mezouar, M., 2011. Solidus and liquidus profiles of chondritic mantle: Implication for melting of the Earth across its history. Earth and Planetary Science Letters 304, 251–259.

Asahara, Y., Frost, D.J., Rubie, D.C., 2007. Partitioning of FeO between magnesiowüstite and liquid iron at high pressures and temperatures : Implications for the composition of the Earth ' s outer core. Earth and Planetary Science Letters 257, 435–449.

Badro, J., Aubert, J., Hirose, K., Nomura, R., Blanchard, I., Borensztajn, S., Siebert, J., 2018. Magnesium partitioning between Earth's mantle and core and its potential to drive an early exsolution geodynamo. Geophysical Research Letters 45, 13,240–13,248.

Badro, J., Brodholt, J.P., Piet, H., Siebert, J., Ryerson, F.J., 2015. Core formation and core composition from coupled geochemical and geophysical constraints. Proceedings of the National Academy of Sciences of the United States of America 112, 12310–4.

569 Badro, J., Cote, A.S., Brodholt, J.P., 2014. A seismologically consistent
570 compositional model of Earth's core. Proceedings of the National Academy
571 of Sciences 111, 7542–7545.

572 Badro, J., Siebert, J., Nimmo, F., 2016. An early geodynamo driven by
573 exsolution of mantle components from Earth's core. Nature 536, 326–328.

574 Benedetti, L.R., Loubeyre, P., 2004. Temperature gradients, wavelength-
575 dependent emissivity, and accuracy of high and very-high temperatures
576 measured in the laser-heated diamond cell. High Pressure Research 24,
577 423–445.

578 Blanchard, I., Siebert, J., Borensztajn, S., Badro, J., 2017. The solubility of
579 heat-producing elements in Earth's core. Geochemical Perspectives Letters
580 5, 1–5.

581 Bouhifd, M.A., Jephcoat, A.P., 2011. Convergence of Ni and Co metal –
582 silicate partition coef fi cients in the deep magma-ocean and coupled silicon
583 – oxygen solubility in iron melts at high pressures. Earth and Planetary
584 Science Letters 307, 341–348.

585 Braukmüller, N., Wombacher, F., Funk, C., Münker, C., 2019. Earth's
586 volatile element depletion pattern inherited from a carbonaceous chondrite-
587 like source. Nature Geoscience 12, 564–568.

588 Chabot, N.L., Agee, C.B., 2003. Core formation in the Earth and Moon:
589 New experimental constraints from V, Cr, and Mn. Geochimica et Cos-
590 mochimica Acta 67, 2077–2091.

591 Chidester, B.A., Rahman, Z., Righter, K., Campbell, A.J., 2017. Metal-
592 silicate partitioning of U: Implications for the heat budget of the core and
593 evidence for reduced U in the mantle. Geochimica et Cosmochimica Acta
594 199, 1–12.

595 Corgne, A., Keshav, S., Wood, B.J., McDonough, W.F., Fei, Y., 2008. Metal-
596 silicate partitioning and constraints on core composition and oxygen fugac-
597 ity during Earth accretion. Geochimica et Cosmochimica Acta 72, 574–589.

598 Corgne, A., Siebert, J., Badro, J., 2009. Oxygen as a light element: A solution
599 to single-stage core formation. Earth and Planetary Science Letters 288,
600 108–114.

601 Cottrell, E., Walter, M.J., Walker, D., 2009. Metal-silicate partitioning of
602 tungsten at high pressure and temperature: Implications for equilibrium
603 core formation in Earth. Earth and Planetary Science Letters 281, 275–
604 287.

605 Fiquet, G., Auzende, A.L., Siebert, J., Corgne, A., Bureau, H., Ozawa, H.,
606 Garbarino, G., 2010. Melting of Peridotite to 140 Gigapascals. Science
607 329, 1516–1518.

608 Fischer, R.A., Nakajima, Y., Campbell, A.J., Frost, D.J., Harries, D., Lan-
609 genhorst, F., Miyajima, N., Pollok, K., Rubie, D.C., 2015. High pressure
610 metal-silicate partitioning of Ni, Co, V, Cr, Si, and O. Geochimica et
611 Cosmochimica Acta 167, 177–194.

612 Hillgren, V.J., Drake, M.J., Rubie, D.C., 1996. High pressure and high
613 temperature metal-silicate partitioning of siderophile elements: The im-
614 portance of silicate liquid composition. Geochimica et Cosmochimica Acta
615 60, 2257–2263.

616 Huang, D., Badro, J., 2018. Fe-Ni ideality during core formation on Earth.
617 American Mineralogist 103, 1701–1710.

618 Huang, D., Badro, J., Brodholt, J., Li, Y., 2019. Ab Initio Molecular Dynam-
619 ics Investigation of Molten Fe–Si–O in Earth's Core. Geophysical Research
620 Letters 46, 6397–6405.

621 Huang, D., Badro, J., Siebert, J., 2020. The niobium and tantalum concentra-
622 tion in the mantle constrains the composition of earth's primordial magma
623 ocean. Proceedings of the National Academy of Sciences 117, 27893–27898.

624 Jana, D., Walker, D., 1997a. The impact of carbon on element distribution
625 during core formation. Geochimica et Cosmochimica Actamica et 61, 2759–
626 2763.

627 Jana, D., Walker, D., 1997b. The influence of silicate melt composition on
628 distribution of siderophile elements among metal and silicate liquids. Earth
629 and Planetary Science Letters 150, 463–472.

630 Jana, D., Walker, D., 1997c. The influence of sulfur on partitioning of
631 siderophile elements. Geochimica et Cosmochimica Acta 61, 5255–5277.

Jennings, E., Jacobson, S., Rubie, D., Nakajima, Y., Vogel, A., Rose-Weston, L., Frost, D., 2021. Metal–silicate partitioning of w and mo and the role of carbon in controlling their abundances in the bulk silicate earth. Geochimica et Cosmochimica Acta 293, 40–69.

JSPSNCS, 1988. Steelmaking data sourcebook. Rev. ed., New York : Gordon and Breach Science Publishers.

Karki, B.B., Bhattarai, D., Mookherjee, M., Stixrude, L., 2010. Visualization-based analysis of structural and dynamical properties of simulated hydrous silicate melt. Physics and Chemistry of Minerals 37, 103–117.

Kleine, T., Münker, C., Mezger, K., Palme, H., 2002. Rapid accretion and early core formation on asteroids and the terrestrial planets from Hf-W chronometry. Nature 418, 952–955.

Kubik, E., Siebert, J., Blanchard, I., Agranier, A., Mahan, B., Moynier, F., 2021. Earth's volatile accretion as told by cd, bi, sb and tl core–mantle distribution. Geochimica et Cosmochimica Acta .

Li, J., Agee, C.B., 1996. Geochemistry of mantle–core differentiation at high pressure. Nature 381, 686–689.

Ma, Z., 2001. Thermodynamic description for concentrated metallic solutions using interaction parameters. Metallurgical and Materials Transactions B 32, 87–103.

Mahan, B., Siebert, J., Blanchard, I., Borensztajn, S., Badro, J., Moynier, F., 2018. Constraining compositional proxies for earth's accretion and core formation through high pressure and high temperature zn and s metal-silicate partitioning. Geochimica et Cosmochimica Acta 235, 21–40.

McDonough, W., Sun, S.s., 1995. The composition of the earth. Chemical Geology 120, 223–253.

Mcdonough, W.F., 2003. Compositional Model for the Earth's Core. Treatise On Geochemistry 2, 547–568.

Mysen, B., 1983. The Structure of silicate melts. Annual Review of Earth and Planetary Sciences 11, 75–97.

O'Neill, H.S.C., Berry, A.J., 2006. Activity coefficients at low dilution of CrO, NiO and CoO in melts in the system CaO-MgO-Al2O3-SiO2 at 1400C: Using the thermodynamic behaviour of transition metal oxides in silicate melts to probe their structure. Chemical Geology 231, 77–89.

O'Neill, H.S.C., Eggins, S.M., 2002. The effect of melt composition on trace element partitioning: An experimental investigation of the activity coefficients of FeO, NiO, CoO, MoO2 and MoO3 in silicate melts. Chemical Geology 186, 151–181.

Palme, H., O'Neill, H., 2014. Cosmochemical Estimates of Mantle Composition, in: Treatise on Geochemistry: Second Edition. 2nd ed.. Elsevier Ltd.. volume 3, pp. 1–39.

Pozzo, M., Davies, C., Gubbins, D., Alfè, D., 2013. Transport properties for liquid silicon-oxygen-iron mixtures at Earth's core conditions. Physical Review B - Condensed Matter and Materials Physics 87, 1–10.

Raymond, S.N., Brien, D.P.O., Morbidelli, A., Kaib, N.A., 2009. Building the terrestrial planets : Constrained accretion in the inner Solar System. Icarus 203, 644–662.

Ricolleau, A., Fei, Y., Corgne, A., Siebert, J., Badro, J., 2011. Oxygen and silicon contents of Earth's core from high pressure metal-silicate partitioning experiments. Earth and Planetary Science Letters 310, 409–421.

Righter, K., Danielson, L.R., Pando, K.M., Shofner, G.A., Sutton, S.R., Newville, M., Lee, C.T., 2016. Valence and metal/silicate partitioning of Mo: Implications for conditions of Earth accretion and core formation. Earth and Planetary Science Letters 437, 89–100.

Righter, K., Drake, M., Yaxley, G., 1997. Prediction of siderophile element metal-silicate partition coefficients to 20 GPa and 2800°C: the effects of pressure, temperature, oxygen fugacity, and silicate and metallic melt compositions. Physics of the Earth and Planetary Interiors 100, 115–134.

Righter, K., Pando, K.M., Danielson, L., Lee, C.T., 2010. Partitioning of Mo, P and other siderophile elements (Cu, Ga, Sn, Ni, Co, Cr, Mn, V, and W) between metal and silicate melt as a function of temperature and silicate melt composition. Earth and Planetary Science Letters 291, 1–9.

Righter, K., Shearer, C.K., 2003. Magmatic fractionation of Hf and W: Constraints on the timing of core formation and differentiation in the Moon and Mars. Geochimica et Cosmochimica Acta 67, 2497–2507.

Ringwood, A.E., 1959. On the chemical evolution and densities of the planets. Geochemica et Cosmochimica Acta 15, 257–283.

Ringwood, A.E., 1966. Chemical evolution of the terrestrial planets. Geochimica et Cosmochimica Acta 30, 41–104.

Rubie, D.C., Gessmann, C.K., Frost, D.J., 2004. Partitioning of oxygen during core formation on the Earth and Mars. Nature 429, 58–61.

Rubie, D.C., Jacobson, S.A., Morbidelli, A., Brien, D.P.O., Young, E.D., Vries, J.D., Nimmo, F., Palme, H., Frost, D.J., 2015. Accretion and differentiation of the terrestrial planets with implications for the compositions of early-formed Solar System bodies and accretion of water. ICARUS 248, 89–108.

Schönbächler, M., Carlson, R.W., Horan, M.F., Mock, T.D., Hauri, E.H., 2010. Heterogeneous accretion and the moderately volatile element budget of earth. Science 328, 884–887.

Shofner, G.A., Campbell, A.J., Danielson, L.R., Rahman, Z., Righter, K., 2014. Metal-silicate partitioning of tungsten from 10 to 50 GPa, in: 45th Lunar and Planetary Science Conference, p. 1267.

Siebert, J., Badro, J., Antonangeli, D., Ryerson, F.J., 2012. Metal-silicate partitioning of Ni and Co in a deep magma ocean. Earth and Planetary Science Letters 321-322, 189–197.

Siebert, J., Badro, J., Antonangeli, D., Ryerson, F.J., 2013. Terrestrial Accretion Under Oxidizing Conditions. Science 339, 1194–1197.

Siebert, J., Corgne, A., Ryerson, F.J., 2011. Systematics of metal-silicate partitioning for many siderophile elements applied to Earth's core formation. Geochimica et Cosmochimica Acta 75, 1451–1489.

Suer, T.a., Siebert, J., Remusat, L., Menguy, N., Fiquet, G., 2017. A sulfur-poor terrestrial core inferred from metal–silicate partitioning experiments. Earth and Planetary Science Letters 469, 84–97.

726 Thibault, Y., Walter, M.J., 1995. The influence of pressure and temperature
727 on the metal-silicate partition coefficients of nickel and cobalt in a model
728 C1 chondrite and implications for metal segregation in a deep magma
729 ocean. Geochimica et Cosmochimica Acta 59, 991–1002.

730 Tuff, J., Wood, B.J., Wade, J., 2011. The effect of Si on metal-silicate
731 partitioning of siderophile elements and implications for the conditions of
732 core formation. Geochimica et Cosmochimica Acta 75, 673–690.

733 Wade, J., Wood, B., 2005. Core formation and the oxidation state of the
734 Earth. Earth and Planetary Science Letters 236, 78–95.

735 Wade, J., Wood, B.J., Tuff, J., 2012. Metal-silicate partitioning of Mo and W
736 at high pressures and temperatures: Evidence for late accretion of sulphur
737 to the Earth. Geochimica et Cosmochimica Acta 85, 58–74.

738 Walker, D., Agee, C.B., 1989. Partitioning "equilibrium", temperature gra-
739 dients , and constraints on Earth differentiation. Earth and Planetary
740 Science Letters 96, 49–60.

741 Walter, M.J., Thibault, Y., 1995. Partitioning of tungsten and molybdenum
742 between metallic liquid and silicate melt. Science 1345, 13–16.

743 Wood, B.J., Kiseeva, E.S., Mirolo, F.J., 2014. Accretion and core formation:
744 The effects of sulfur on metal-silicate partition coefficients. Geochimica et
745 Cosmochimica Acta 145, 248–267.

746 Wood, B.J., Li, J., Shahar, A., 2013. Carbon in the Core: Its Influence on the
747 Properties of Core and Mantle. Reviews in Mineralogy and Geochemistry
748 75, 231–250.

749 Wood, B.J., Walter, M.J., Wade, J., 2006. Accretion of the Earth and seg-
750 regation of its core. Nature 441, 825–833.

751 Yin, Q., Jacobsen, S.B., Yamashita, K., Blichert-Toft, J., Telouk, P., Al-
752 barède, F., 2002. A short timescale for terrestrial planet formation from
753 Hf-W chronometry of meteorites. Nature 418, 949–952.

Declaration of interests

☒ The authors declare that they have no known competing financial interests or personal relationships that could have appeared to influence the work reported in this paper.

☐The authors declare the following financial interests/personal relationships which may be considered as potential competing interests:
